

High-order plasmon resonances in an Ag/Al₂O₃ core/shell nanorice*

Chen Li(陈立)^{a)b)}, Wei Hong(魏红)^{b)}, Chen Ke-Qiu(陈克求)^{a)}, and Xu Hong-Xing(徐红星)^{b)c)†}

^{a)}Department of Applied Physics, Hunan University, Changsha 410082, China

^{b)}Beijing National Laboratory for Condensed Matter Physics and Institute of Physics, Chinese Academy of Sciences, Beijing 100190, China

^{c)}Center for Nanoscience and Nanotechnology, and School of Physics and Technology, Wuhan University, Wuhan 430072, China

(Received 20 August 2013; revised manuscript received 18 September 2013; published online 20 December 2013)

Using numerical simulation, we investigate the high-order plasmon resonances in individual nanostructures of an Ag nanorice core surrounded by an Al₂O₃ shell. The peak positions of localized surface plasmon resonances (LSPRs) are red-shifted exponentially with the increase of the dielectric shell thickness. This is due to the exponential decay of electromagnetic field intensity in the direction perpendicular to the interface. This exponential red-shift depends on the wavelength of the resonance peak instead of the resonance order. In addition, we find that the LSPRs in an Ag nanorice of 60-nm width can be perfectly described by a single linear function. These features make nanorice an ideal platform for sensing applications.

Keywords: localized surface plasmon resonances, nanorice, core-shell, LSPR sensing

PACS: 73.20.Mf, 78.67.-n, 42.25.-p

DOI: 10.1088/1674-1056/23/2/027303

1. Introduction

Noble metal nanostructures have many fascinating optical properties depending on their shapes, sizes, compositions and surrounding media.^[1–5] Metallic nanoparticles (MNPs) have been extensively investigated in nanophotonics due to their highly tunable localized surface plasmon resonances (LSPRs).^[6] MNPs can be widely used as ultrasensitive probes for local chemical or biological sensing due to the strong dependence of their LSPRs on the environment.^[7–9] Meanwhile, the enormous electromagnetic field enhancement induced by LSPRs makes them ideal amplifiers for many weak optical processes, such as surface-enhanced spectroscopy, high harmonic generation, etc.^[10–15]

Recently, the investigations on high-order resonance modes observed in large MNPs beyond a quasi-static limit have attracted increasing attention.^[16–20] Compared with the dipolar resonance, high-order resonances have narrower linewidths because of the reduced radiative damping, resulting in higher Q factors.^[21,22] On the other hand, the investigations on quasi-one-dimensional nanostructures are also very important for the understanding of localized surface plasmons and propagating surface plasmons. Short quasi-one-dimensional nanostructures, like nanorods and nanorice, act as localized surface plasmon resonators. If their length increases to a scale much larger than the wavelength, they work as a waveguide supporting the propagation of surface plasmon waves. The transition from localized surface plasmons to propagating surface plasmons would take place.^[23] In applications, a

dielectric shell is often used as a protective layer or spacer layer. Sometimes a dielectric shell can be generated around the MNPs by adsorbing molecules in the test solution. Therefore, studies on the influences of dielectric shell on the LSPRs in quasi-one-dimensional metallic nanostructures are important for applying them to sensing and detection.

The plasmon resonances of small metallic core/shell nanoparticles have been widely investigated, both experimentally and theoretically.^[24–29] The extended Mie theory can accurately describe the optical properties of single spheroidal particles^[30] or spherical core/shell particles.^[27–29,31] However, the theory cannot be used with nonspherical core/shell particles. It is also difficult to calculate the core/shell MNPs of a wavelength-comparable scale by the normal numerical methods, such as the discrete dipole approximation method and the finite difference time domain method. This is because such large particles within the thin shell layer require a huge number of meshes, which challenge the memory and time needed for the calculations.

In this work, we study the modulation of LSPRs in an individual Ag nanorice surrounded by an Al₂O₃ shell by combining the finite element method (FEM) and the boundary element method (BEM). We show that with the increase of shell thickness, the LSPRs are red-shifted exponentially due to the fact that the intensity of the electromagnetic field exponentially decays along the direction perpendicular to the interface. This exponential red-shift is unrelated to the resonance order but dependent on the resonance wavelength. We further find

*Project supported by the National Key Basic Research and Development Program of China (Grant Nos. 2009CB930700 and 2012YQ12006005), the National Natural Science Foundation of China (Grant Nos. 11134013, 11227407, and 11004237), and the Knowledge Innovation Project of the Chinese Academy of Sciences (Grant No. KJCX2-EW-W04).

†Corresponding author. E-mail: hxxu@iphy.ac.cn

that the LSPRs in an Ag nanorice with a width of 60 nm can be perfectly described by a single linear function.

2. Theoretical method

We combine the finite element method (FEM) and the boundary element method (BEM) to perform the simulations. The commercial COMSOL multiphysics software package (based on FEM) is used for providing the charge distributions and mode analysis. The calculations of LSPRs spectra are mainly based on the BEM.^[32] In the BEM, only the interface between different media should be meshed, thus the mesh number is significantly reduced.

The structure we used in this paper is Ag/Al₂O₃ core/shell nanorice embedded in water as schematically shown in Fig. 1(a). The nanorice is modeled as a prolate spheroid. Parameters r_1 and r_2 are the radii of major and minor axes of the Ag nanorice core, with corresponding length $L = 2r_1$ and width $W = 2r_2$. Parameter d is the thickness of the Al₂O₃ shell. The permittivity of Ag is taken from the experimental data reported by Johnson and Christy,^[33] and the refractive indices of Al₂O₃ and water are set to be 1.7762^[34] and 1.33, respectively. The incident light is plane wave ($\mathbf{E}_i = e_i E_i e^{i\mathbf{k}_i \cdot \mathbf{r} - i\omega t}$, where e_i is the unit vector of electric field) in xz plane, as schematically shown in Fig. 1(b), where θ is the incident angle and φ is the angle between the polarization and xz plane. In a real system, the particles are randomly arranged, so here we set $\theta = 45^\circ$ and $\varphi = \arctan(1/\sqrt{2})$ to ensure that the components of exciting field satisfy $E_{i,x} = E_{i,y} = E_{i,z}$. This kind of setting ensures that all resonance modes have the possibility to be excited.

3. Results and discussion

First, by using the commercial COMSOL multiphysics software package based on FEM, we calculate the extinction and absorption cross section spectra of the Ag/Al₂O₃ core/shell nanorice with $L = 300$ nm, $W = 60$ nm, and $d = 15$ nm, as shown in Fig. 1(c). Three resonance peaks (1279 nm, 770 nm, and 604 nm) are shown in the visible-near infrared, corresponding to three different resonance modes. To confirm the orders of these three modes, we plot the corresponding surface charge distributions as shown in Fig. 1(d). The longitudinal LSPRs in the quasi-one-dimensional structure can be viewed as Fabry–Pérot resonance along the long axis and reflected at the terminals.^[35] With this consideration, we define the order of these three resonance modes as $m = 1$, $m = 2$, and $m = 3$. Recent studies have also shown that an asymmetric Fano line-shape may appear in the scattering spectrum of a single rod-shape MNP, originating from the interference between different modes.^[36,37] Here we find similar asymmetric line shapes in the extinction spectrum and asymmetric surface charge distributions for the order of $m = 2$

and 3 as shown in Figs. 1(c) and 1(d). Figure 1(c) also shows that the linewidth of the multipolar plasmon resonance is much narrower than that of the dipolar mode, which results in higher quality factor Q , e.g. Q is about 6 for $m = 1$, but increases to around 23 for $m = 2$ and 36 for $m = 3$. The quality factor is obtained by $Q = \omega_m/\Gamma$, where ω_m and Γ are the resonance energy and the full width at half maximum of the LSPR peak, respectively. The high quality factors of the multipolar plasmon resonances are of critical importance in many LSPR-based applications.

One of the most important properties of MNPs is the strong dependence of LSPRs on the dielectric environment. The existence of Al₂O₃ shell changes the polarization characteristics of the free electrons in the metal surface, resulting in a peak position shift of LSPR. To understand this dependence, we calculate the LSPRs in an individual Ag nanorice with Al₂O₃ shell of different thickness values embedded in water. The following simulations are performed by using BEM. Results are shown in Fig. 2, where the length and the width of the Ag nanorice are kept at $L = 400$ nm and $W = 60$ nm. As shown in Fig. 2(a), five LSPR peaks can be observed and all of them are red-shifted as d increases. As is well known, the LSPRs of individual MNP are red-shifted as the refractive index of the surrounding medium increases. Here the existence of a high refractive index dielectric shell increases the effective refractive index of the medium surrounding the nanorice. Figure 2(b) shows the resonance peak positions, each as a function of the shell thickness and their corresponding fitting curves. The resonance peaks are red-shifted rapidly when the shell thickness d is small. With the increase of d , the shift gradually slows down. Finally the resonance peak positions become almost constant. Curve fitting reveals that this kind of red-shift follows an exponential function in the form of

$$\lambda_m(d) = y_0 - A_0 e^{-d/\tau}.$$

Fitting results are listed in Table 1. From this function we can easily find that

$$\lambda_m(0) = y_0 - A_0$$

is the resonance wavelength of the Ag nanorice without shell and $\lambda_m(\infty) = y_0$ is the resonance wavelength of the Ag nanorice embedded in bulk Al₂O₃. Parameter τ is the exponential factor related to the sensitivity of localized surface plasmon resonances to shell thickness. Figure 2(c) shows the wavelength shift per thickness unit ($\Delta\lambda_m/\Delta d$) for $m = 1-5$ modes, which represents the sensitivity of localized surface plasmon resonances to the change of shell thickness. Obviously, this sensitivity decreases with the increase of d . For the bare Ag nanorice, all resonance modes show a peak shift of more than 6 nm for the coating of 1-nm Al₂O₃ which can be roughly equivalent to a layer of adsorbed molecules in sensing applications.^[38] For the same d , lower order LSPRs have

higher sensitivities, while we should notice that the resonances of different orders occur at different wavelengths. In fact, further investigations indicate that the sensitivity is related to the resonance wavelength rather than resonance order for a

nanorice of different sizes, which will be explained later in this paper. Another feature in Fig. 2(c) is that the sensitivity of the dipolar mode ($m = 1$) is much higher than those of the other modes due to the low resonance energy, i.e. long wavelength.

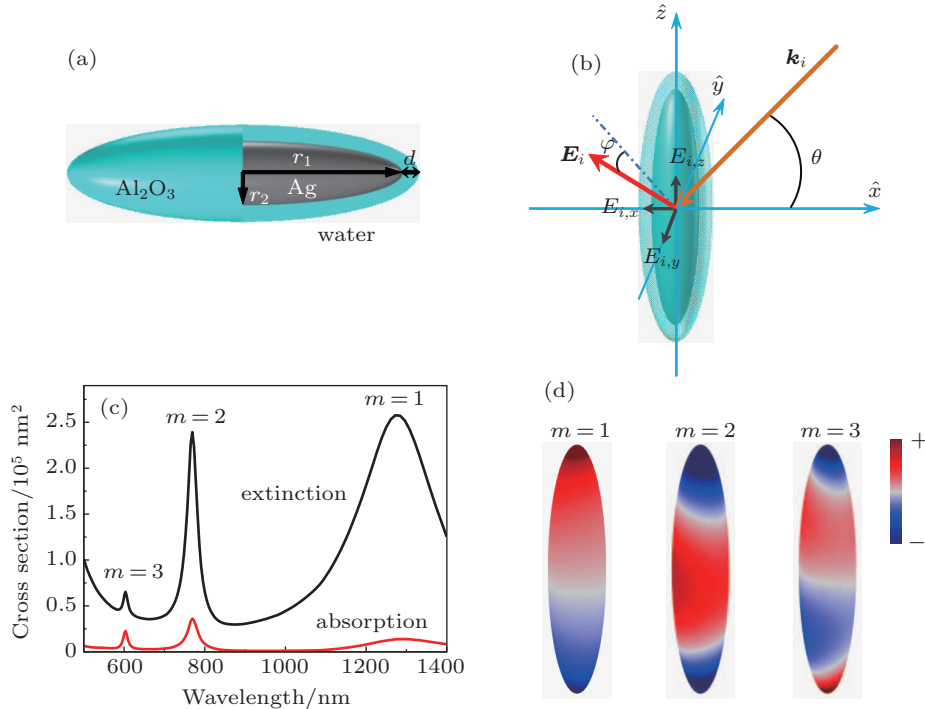


Fig. 1. (color online) (a) and (b) Schematic sketches of the MNP geometry used for theoretical calculations, with $\theta = 45^\circ$ and $\varphi = \arctan(1/\sqrt{2})$ (φ is the angle between polarization and xz plane). (c) The extinction and absorption cross section simulated by using the commercial COMSOL multiphysics software package based on FEM. Here, $L = 2r_1 = 300$ nm, $W = 2r_2 = 60$ nm, and $d = 15$ nm. (d) The surface charge distributions on the metal surface corresponding to the resonance peaks of 1279 nm for $m = 1$, 770 nm for $m = 2$, and 604 nm for $m = 3$.

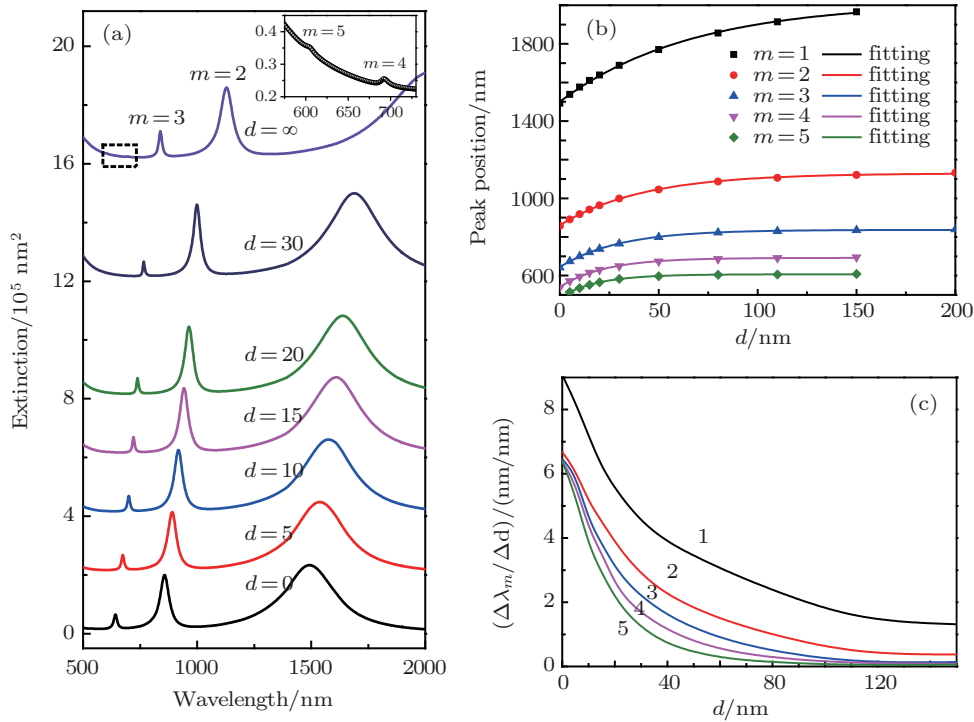


Fig. 2. (color online) (a) Extinction spectra of an individual Ag nanorice with different thickness values of Al_2O_3 shell in water. The length and width of the Ag nanorice are $L = 400$ nm and $W = 60$ nm. $d = \infty$ nm means that the Ag nanorice is embedded in Al_2O_3 medium. (b) The resonance peak positions (dots) as a function of the thickness d and their corresponding fitting curves (solid) in the form of $\lambda_m(d) = \gamma_0 - A_0 e^{-d/\tau}$. Fitting results are listed in Table 1. (c) The plots of resonance wavelength shift per thickness unit ($\Delta\lambda_m/\Delta d$) generated from the calculation data shown in panel (b) versus thickness d .

Table 1. Fitting results to the exponential expression $\lambda_m(d) = y_0 - A_0 e^{-d/\tau}$ in Fig. 2(b).

Mode order	y_0	A_0	τ
$m = 1$	2014.38 ± 9.80	513.7 ± 8.75	66.3 ± 2.97
$m = 2$	1129.49 ± 2.14	269 ± 2.49	42.3 ± 1.16
$m = 3$	836.7 ± 0.97	193.2 ± 1.43	29.7 ± 0.58
$m = 4$	691.6 ± 1.15	151 ± 1.74	22.8 ± 0.64
$m = 5$	606.6 ± 0.57	119.4 ± 1.54	19.06 ± 0.48

A simple planar waveguide model can be used to gain a deeper understanding about the origin of this exponential dependence. We consider the fundamentals of surface plasmon polaritons at an infinite flat metal/dielectric interface with Ag on one side and H₂O on the other side. The electric field can be

$$e^{-2dk_{z,\text{Al}_2\text{O}_3}} = \frac{k_{z,\text{Al}_2\text{O}_3}/\epsilon_{\text{Al}_2\text{O}_3} + k_{z,\text{Ag}}/\epsilon_{\text{Ag}}}{k_{z,\text{Al}_2\text{O}_3}/\epsilon_{\text{Al}_2\text{O}_3} - k_{z,\text{Ag}}/\epsilon_{\text{Ag}}} \frac{k_{z,\text{Al}_2\text{O}_3}/\epsilon_{\text{Al}_2\text{O}_3} + k_{z,\text{H}_2\text{O}}/\epsilon_{\text{H}_2\text{O}}}{k_{z,\text{Al}_2\text{O}_3}/\epsilon_{\text{Al}_2\text{O}_3} - k_{z,\text{H}_2\text{O}}/\epsilon_{\text{H}_2\text{O}}}.$$

We cannot obtain the analytical solution of $k_{z,j}$ directly, but we can know that $k_{z,j}$ is exponentially dependent on d . $k_{z,j}^2 = k_{x,j}^2 - k_0^2 \epsilon_j$, so the wave vector along the interface $k_{x,j}$ is also exponentially dependent on thickness d . Figure 3(c) shows the numerical results of $k_{x,j}$ at $\lambda_0 = 633$ nm for different values of Al₂O₃ thickness d , which shows an exponential dependence. If we cut this planar multilayer waveguide into a cavity with two reflection mirrors, the resonant mode occurs when $L'k_{x,j}/\pi = m$, where L' is the length of the cavity and m is an integer. For planar waveguide, $k_{x,j}$ is proportional to k_0 .^[39] For fixed L' and m , a decrease of k_0 is needed for the increased d to ensure that the resonance occurs, which means that the

described as $\mathbf{E}_j = (E_{x,j}, 0, E_{z,j}) e^{i(k_{x,j}x - \omega t)} e^{-k_{z,j}z}$, where $k_{z,j}$ ($j = \text{Ag}, \text{H}_2\text{O}$) is the component of the wave vector perpendicular to the interface of the two media, and $k_{x,\text{Ag}} = k_{x,\text{H}_2\text{O}}$ is the component of the wave vector along the interface. The electric field exponentially decays in the z direction, as shown in Fig. 3(a), which is obtained by the mode-analysis module in COMSOL multiphysics software. If there is an additional Al₂O₃ layer of thickness d on the metal surface, this exponential decay trend is more or less maintained as shown in Fig. 3(b). A similar exponential decay can be found in the nanorice as shown in the insets of Figs. 3(a) and 3(b). Solving the wave vector of this system results in an expression containing the thickness d in the exponential form^[39]

resonance wavelength $\lambda_m = 2\pi/k_0$ is red-shifted. Therefore, the exponential dependence of $k_{x,j}$ on the thickness d of Al₂O₃ layer results in a corresponding exponential shift of resonance peak positions λ_m . A similar exponential dependence of $k_{x,j}$ on shell thickness can be found in a core/shell nanowire system (not shown here). So in principle, we can use this idea in quasi-one-dimensional systems like nanorice and nanorod. That is why the LSPR peak position λ_m in Fig. 2 is red-shifted exponentially with the increase of the thickness of the Al₂O₃ shell. We also simulate the nanorod core/shell system which produces a similar exponential red-shift (not shown here).

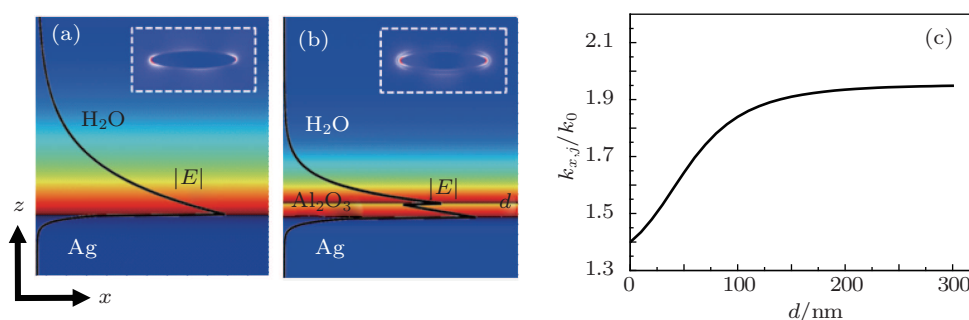


Fig. 3. (color online) ((a), (b)) The electric field intensity maps of a surface plasmon wave in planar waveguide without (a) and with (b) Al₂O₃ layer, with the vacuum wavelength of incident light $\lambda_0 = 633$ nm and the thickness of Al₂O₃ layer $d = 70$ nm. The solid black curves represent exponential dependences of the electromagnetic field intensity on the distance away from the interface in panels (a) and (b), respectively. The insets show the electric field intensity distributions of $m = 2$ mode in an Ag nanorice without (a) and with (b) Al₂O₃ shell. (c) The dependence of wave vector $k_{x,j}$ on Al₂O₃ thickness for the planar waveguide shown in panel (b), with $\lambda_0 = 633$ nm and vacuum wave vector $k_0 = 2\pi/\lambda_0$. An exponential dependence of $k_{x,j}$ on d can be clearly observed.

Since the LSPR of the MNP depends sensitively on its aspect ratio,^[40] the resonance peak positions of different modes can be shifted to the same wavelength by changing the length of the Ag nanorice as shown in Fig. 4(a). Four overlapped peak positions are marked as I, II, III, and IV, corresponding to I:

$m = 1$ mode for $L = 300$ nm and $m = 2$ mode for $L = 600$ nm; II: $m = 2$ for $L = 400$ nm and $m = 3$ for $L = 600$ nm; III: $m = 2$ for $L = 300$ nm and $m = 4$ for $L = 600$ nm; IV: $m = 3$ mode for $L = 300$ nm and $m = 4$ mode for $L = 400$ nm. Interestingly, with shell thickness d increasing from 0 nm to

200 nm, these four overlapped peak positions remain overlapped, which means that the influence of the shell is independent of the resonance order (see Fig. 4(b)). This is because the shift of the resonance peaks induced by a dielectric shell depends on the localization of surface plasmons along the direction perpendicular to the metal surface, which is wavelength-sensitive but independent of resonance order. The overlapped

peak positions for modes of different orders in Fig. 4(b) also mean that the sensitivity $\Delta\lambda_m/\Delta d$ is only dependent on resonance wavelength. In sensing applications, we can directly obtain the information about the environment from the LSPR wavelength without considering the resonance order. The overlap for peak I in Fig. 4(b) is not perfect because of the strong radiative damping of $m = 1$ mode.^[21]

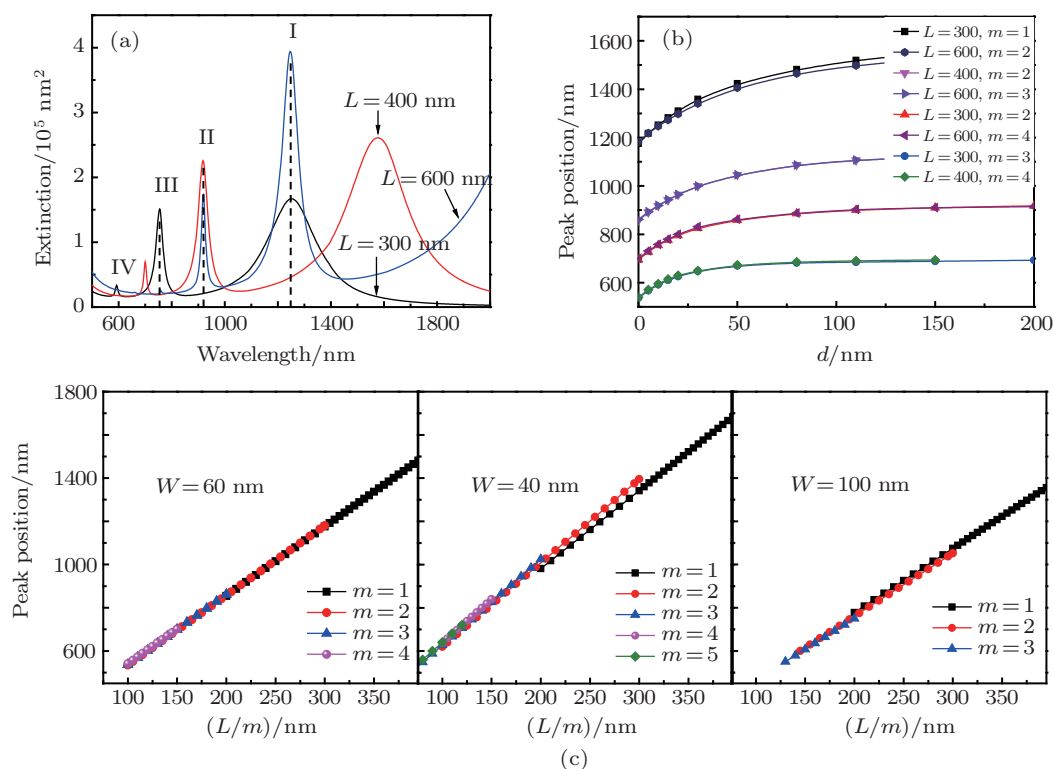


Fig. 4. (color online) (a) Extinction spectra of Ag/Al₂O₃ core/shell nanorice ($W = 60$ nm, $d = 10$ nm) of different lengths ($L = 300$ nm, 400 nm, and 600 nm). The surrounding medium is water. Four overlapped peaks are marked as I, II, III, and IV. (b) Plots of positions of overlapped peaks in panel (a) versus Al₂O₃ thickness d . (c) Plots of the resonance peak positions of Ag nanorice with different lengths versus L/m . Here, L is the physical length of the Ag nanorice, m is the resonance order, W is the width of the nanorice, and $d = 0$ nm.

Traditional antenna design makes use of a structure with a characteristic length L that is directly related to the wavelength λ of the incoming (or outgoing) radiation ($L = \lambda/2$ for an ideal half-wave dipole antenna).^[41] Here for the LSPRs in the quasi-one-dimensional nanorice, we can use effective surface plasmon wavelength $\lambda_{\text{eff}} = C\lambda$ instead of external wavelength, where C is coefficient related to a short-axis radius and dielectric properties.^[42] Considering the shift of resonance modes induced by terminal reflection, the characteristic length can be described by effective length $L_{\text{eff}} = L + L_c$, where L is the physical length and L_c is the extended cavity length.^[35,43,44] The resonance condition becomes $L_{\text{eff}} = L + L_c = m\lambda_{\text{eff}}/2$. Then we have the resonance wavelength for the m order mode, i.e. $\lambda_m = \lambda_{\text{eff}}/C = 2(L/m + L_c/m)/C$. The numerical calculation results are shown in Fig. 4(c). We find that the LSPR peak positions in an Ag nanorice with a width of 60 nm can be described by a simple linear function ($\lambda_m = 3.175L/m + 222$),

i.e. L_c/m keeps constant. Taking the overlapped peak II in Fig. 4(a) for example, we obtain $\lambda_{\text{eff}}/2 = (L + L_c)/m = (400 + L'_c)/2 = (600 + L''_c)/3$, i.e. $L'_c/2 = L''_c/3$. More calculations show that for an Ag nanorice of $W = 40$ nm, $\lambda_{m+1} > \lambda_m$ at the same L/m , which means that L_c/m increases with m increasing; while for an Ag nanorice of $W = 100$ nm, $\lambda_{m+1} < \lambda_m$ at the same L/m , i.e., L_c/m decreases with the increase of resonance order m . We believe that this shift arises from the non-uniform short-axis radius which makes the surface plasmon wave non-uniform.^[17,45] In the Ag nanowire system, the plasmon wavelength decreases with the decrease of the nanowire radius.^[46] Here in our system, the Ag nanorice can be regarded as a waveguide consisting of many parts with different radii ranging from $W/2$ to 0 nm along the long axis. Segments of different radii will make the values of the correction term L_c , effective cavity length, different. That is why L_c/m shows different dependences on resonance order m for $W = 40$ nm,

60 nm or 100 nm. This feature of L_c/m is totally different from that in a nanorod. For a cylindrical nanorod with radius R and hemispherical ends, the uniform radius distribution makes the extended cavity length L_c an approximate constant value $2R$, i.e. L_c/m always decreases with the increase of resonance order m .^[42–44]

4. Conclusions

In this paper, we derived an exponential red-shift of the LSPR peak position of an Ag nanorice with the increase of the dielectric shell thickness, due to the exponential localization of surface plasmons on the metal surface. This exponential dependence is independent of the resonance order but related to the wavelength, which makes nanorice an ideal platform for LSPR sensing. We can detect the thickness of the dielectric shell and other environment information around the core/shell MNPs through the exponential red-shift of LSPR peaks without considering the resonance order. In addition, we find that the dependences of LSPR peak positions on L/m of different resonance orders in an Ag nanorice can be easily designed in a common linear form. These features can be useful for LSPR sensing applications.

Acknowledgment

The authors thank Prof. Javier Aizpurua for generously providing the BEM codes.

References

- [1] Kelly K L, Coronado E, Zhao L L and Schatz G C 2003 *J. Phys. Chem. B* **107** 668
- [2] Hutter E and Fendler J H 2004 *Adv. Mater.* **16** 1685
- [3] Noguez C 2007 *J. Phys. Chem. C* **111** 3806
- [4] Shuford K L, Lee J, Odom T W and Schatz G C 2008 *J. Phys. Chem. C* **112** 6662
- [5] Wang J F, Li H J, Zhou Z Y, Li X Y, Liu J and Yang H Y 2010 *Chin. Phys. B* **19** 117310
- [6] Pelton M, Aizpurua J and Bryant G 2008 *Laser & Photon. Rev.* **2** 136
- [7] Willets K A and Van Duyne R P 2007 *Ann. Rev. Phys. Chem.* **58** 267
- [8] Stewart M E, Anderton C R, Thompson L B, Maria J, Gray S K, Rogers J A and Nuzzo R G 2008 *Chem. Rev.* **108** 494
- [9] Mayer K M and Hafner J H 2011 *Chem. Rev.* **111** 3828
- [10] Xu H X, Bjerneld E J, Kall M and Borjesson L 1999 *Phys. Rev. Lett.* **83** 4357
- [11] Xu H X, Aizpurua J, Kall M and Apell P 2000 *Phys. Rev. E* **62** 4318
- [12] Aizpurua J, Bryant G W, Richter L J, de Abajo F J G, Kelley B K and Mallouk T 2005 *Phys. Rev. B* **71** 235420
- [13] Muskens O L, Giannini V, Sanchez-Gil J A and Rivas J G 2007 *Nano Lett.* **7** 2871
- [14] Kim S, Jin J H, Kim Y J, Park I Y, Kim Y and Kim S W 2008 *Nature* **453** 757
- [15] Shi X Z, Shen C M, Wang D K, Li C, Tian Y, Xu Z C, Wang C M and Gao H J 2011 *Chin. Phys. B* **20** 076103
- [16] Krenn J R, Schider G, Rechberger W, Lamprecht B, Leitner A, Aussenegg F R and Weeber J C 2000 *Appl. Phys. Lett.* **77** 3379
- [17] Wei H, Reyes-Coronado A, Nordlander P, Aizpurua J and Xu H X 2010 *ACS Nano* **4** 2649
- [18] Lee Y H, Chen H J, Xu Q H and Wang J F 2011 *J. Phys. Chem. C* **115** 7997
- [19] Lopez-Tejiera F, Paniagua-Dominguez R and Sanchez-Gil J A 2012 *ACS Nano* **6** 8989
- [20] Kazuma E and Tatsuma T 2013 *J. Phys. Chem. C* **117** 2435
- [21] Stockman M I 2011 *Opt. Express* **19** 22029
- [22] Zhang S P, Chen L, Huang Y Z and Xu H X 2013 *Nanoscale* **5** 6985
- [23] Vesseur E J R, de Waele R, Kuttge M and Polman A 2007 *Nano Lett.* **7** 2843
- [24] Xu H X and Kall M 2002 *Sensor Actuat. B-Chem.* **87** 244
- [25] Whitney A V, Elam J W, Zou S L, Zinovev A V, Stair P C, Schatz G C and Van Duyne R P 2005 *J. Phys. Chem. B* **109** 20522
- [26] Shanthil M, Thomas R, Swathi R S and Thomas K G 2012 *J. Phys. Chem. Lett.* **3** 1459
- [27] Xu H X 2004 *Appl. Phys. Lett.* **85** 5980
- [28] Zhao K, Xu H X, Gu B H and Zhang Z Y 2006 *J. Chem. Phys.* **125** 081102
- [29] Wang W, Li Z P, Gu B H, Zhang Z Y and Xu H X 2009 *ACS Nano* **3** 3493
- [30] Asano S and Yamamoto G 1975 *Appl. Opt.* **14** 29
- [31] Jiang S M, Wu D J, Cheng Y and Liu X J 2012 *Chin. Phys. B* **21** 127806
- [32] de Abajo F J G and Howie A 2002 *Phys. Rev. B* **65** 115418
- [33] Johnson P B and Christy R W 1972 *Phys. Rev. B* **6** 4370
- [34] Hagemann H J, Gudat W and Kunz C 1974 *Optical Constants from the Far Infrared to the X-ray Region* (Hamburg: Deutsches Elektronen-Synchrotron DESY)
- [35] Dorfmler J, Vogelgesang R, Weitz R T, Rockstuhl C, Etrich C, Pertsch T, Lederer F and Kern K 2009 *Nano Lett.* **9** 2372
- [36] Reed J M, Wang H N, Hu W F and Zou S L 2011 *Opt. Lett.* **36** 4386
- [37] Lopez-Tejiera F, Paniagua-Dominguez R, Rodriguez-Oliveros R and Sanchez-Gil J A 2012 *New J. Phys.* **14** 023035
- [38] Raschke G, Kowarik S, Franzl T, Sonnichsen C, Klar T A, Feldmann J, Nichtl A and Kurzinger K 2003 *Nano Lett.* **3** 935
- [39] Maier S A 2007 *Plasmonics: Fundamentals and Applications* (New York: Springer)
- [40] Bryant G W, De Abajo F J G and Aizpurua J 2008 *Nano Lett.* **8** 631
- [41] Milligan T A 2005 *Modern Antenna Design* (New Jersey: John Wiley & Sons)
- [42] Novotny L 2007 *Phys. Rev. Lett.* **98** 266802
- [43] Alù A and Engheta N 2008 *Phys. Rev. Lett.* **101** 043901
- [44] Taminiau T H, Stefani F D and van Hulst N F 2011 *Nano Lett.* **11** 1020
- [45] Liang H Y, Rossouw D, Zhao H G, Cushing S K, Shi H L, Korinek A, Xu H X, Rosei F, Wang W Z, Wu N Q, Botton G A and Ma D L 2013 *J. Am. Chem. Soc.* **135** 9616
- [46] Chang D E, Sørensen A S, Hemmer P R and Lukin M D 2007 *Phys. Rev. B* **76** 035420